ELSEVIER

Contents lists available at ScienceDirect

Journal of Aerosol Science

journal homepage: www.elsevier.com/locate/jaerosci





On the dependence of electrical mobility on temperature, humidity and structure of alkylammonium ions

Xuemeng Chen ^{a,b,*}, Juha Kangasluoma ^c, Jakub Kubečka ^d, Ivo Neefjes ^c, Hanna Vehkamäki ^c, Markku Kulmala ^c, Amirreza Tootchi ^b, Farah Mubas Sirah ^b, Leyan Hua ^b, Carlos Larriba-Andaluz ^b, Heikki Junninen ^a

- ^a Institute of Physics, University of Tartu, W. Ostwaldi 1, EE-50411, Tartu, Estonia
- ^b Department of Mechanical Engineering, IUPUI, Indianapolis, IN, USA
- ^c Institute for Atmospheric and Earth System Research (INAR)/Physics, Faculty of Science, University of Helsinki, Finland
- ^d Department of Chemistry, Aarhus University, Aarhus, Denmark

ARTICLE INFO

Handling Editor: Chris Hogan

ABSTRACT

Insights into the effect of temperature (T) and relative humidity (RH) as well as structure and polarisation on ion mobility help the comparison and interpretation of mobility and mass-based data. We measured alkylammonium ions in air under different T (14 °C, 24 °C, 34 °C and 41 °C) and RH (0 %, 20 %, 40 %) conditions using two individual setups (in both cases a planar differential mobility analyser coupled with a time-of-flight mass spectrometer) and the results are in excellent agreement. Mobility increases with rising T and decreases with water vapour loading. When separating the measurement mobility by structures, clear mass dependence was observed. The measured mobilities exhibited large deviations from theoretically calculated results in dry conditions, which are possibly caused by adduct formation on the monomer ions via clustering (or reactions). This phenomenon seems to be unavoidably associated with light ions under atmospheric pressures, which is worth further exploration and bearing in mind when comparing measurements to calculations. Both methanol and oxygen (occasionally nitrogen or alkyl chain elongation) are possible candidates of the adduct. Under spherical assumption, we used the modified Mason-Schamp's approximation to link the measured mobility to the mobility equivalent diameter. The drag enhancement factor ξ and the effective gas-molecule collision diameter $d_{\rm g}$ derived from our measurement data are comparable to literature values. Our data also exposed a non-linear dependence on the polarisation parameter ε^* . Polarisation, ξ and d_{g} were parameterised using linear models against ion structures, T, and RH for primary, secondary and tertiary alkylammonium ions with identical alkyl groups. Our model parametrisations predict mobilities within ± 10 % deviation from the measured data. The model also has satisfying predicting power for alkylammonium ions with unidentical alkyl structures.

^{*} Corresponding author. Institute of Physics, University of Tartu, W. Ostwaldi 1, EE-50411, Tartu, Estonia. E-mail address: xuemeng015@gmail.com (X. Chen).

1. Introduction

Electrical mobility is an important size-related parameter in describing aerosol particles. It is also powerful in analytical chemistry (where the use of 'ion mobility' is preferred over 'electrical mobility') for ion separation and structural investigation, usually involving the employment of an ion mobility spectrometer (IMS) (Campuzano et al., 2012; Dodds et al., 2017; Gabelica & Marklund, 2018; Dodds & Baker, 2019). Although IMS has been used in several aerosol studies (Oberreit et al., 2014; Krechmer et al., 2016), differential mobility analysers (DMA) and aspiration ion counters that measure the same ion property but through slightly different techniques are more widely applied in this field, especially in atmospheric aerosol studies (Kulmala et al., 2012; Wiedensohler et al., 2012; Mirme & Mirme, 2013) due to their robustness, size range, suitability for continuous measurement, and the convenience of their operation at atmospheric pressure.

Atmospheric aerosol particles affect air quality, human health and climate (Poschl, 2005). Although these effects mostly result from particles of hundreds of nanometres to micron sizes (Ramanathan et al., 2001; von Klot et al., 2005; Atkinson et al., 2015), the majority of these particles are secondary aerosol particles that have origins traceable to gaseous precursors (Curtius, 2006, Kerminen et al., 2018). The process of forming 1–2 nm nanoparticles that can undergo subsequent growth from the gas phase is known as atmospheric new particle formation (NPF) (Kulmala et al., 2014). As NPF occurs in the sub-2 nm range, which is much smaller than the mean free path in air, the process falls in the free-molecular regime. Experimental NPF studies utilise both mobility-based and mass-based instrumentations (Kulmala et al., 2012). The conversion between electric mobility and mass is possible via mass diameter and spherical assumption. However, this is not a straightforward task, as the link depends on a scattering drag enhancement factor, where the size of the gas molecules cannot be neglected (Fernández-García & Fernández de la Mora, 2013). Aside from the physical size of the ion, electrical mobility is also affected by potential interactions between the ion and induced dipoles on surrounding neutral gas molecules in polarisable gas medium, such as air (Kim et al., 2008; Lee et al., 2018). When considering atmospheric measurements, the mobility–mass relation is further complicated by temperature and humidity variations.

In order to reliably compare mobility-based and mass-based data, it is necessary to gain insights into the effects of structure, polarisation, temperature, and humidity on the mobility-mass relation. In this work, we characterise how ion mobility responds to changes in temperature and relative humidity using primary, secondary, and tertiary alkylammonium cations. Alkylammonium ions are protonated amines, some of which are common in ambient air stemming from biogenic and/or anthropogenic sources (Ge et al., 2011; Kieloaho et al., 2013) and are relevant for atmospheric NPF (Almeida et al., 2013; Moller et al., 2020). The different structures of these alkylammonium ions also allow probing the effect of ion conformation on mobility and the polarisation effect in connection to ion structures. By examining the effects of temperature, humidity, ion structures, and polarisation on electrical mobility through laboratory experiments, we aim to parameterise these effects for theoretical ion mobility calculations in the free molecular regime.

2. Methods

Ion mobility measurements were carried out using two individual setups at Indiana University - Purdue University Indianapolis (IUPUI) and the University of Helsinki (UHel). Both setups were composed of a planar differential mobility analyser (DMA) and a Time-of-Flight Mass Spectrometer (ToF MS). Tetrabutylammonium cation (TBA⁺) was used as the calibrant for mobility analysis. Our samples contain alkylammonium cations of linear and branched structures, which allows the characterisation of ion conformation

Table 1
List of studied primary, secondary and tertiary alkyl ammonium cations and their molecular weight and density. 'X' indicates measurement of the corresponding cation performed.

Alkyl(s) of the alkyl-ammonium cations	Molecular weight [Da]	Density [kg/m ³]	IUPUI	UHel	UT
Dimethyl	46.08784	649.6	X	X	
Ethyl	46.08784	688	X	X	
Trimethyl	60.11784	630	X	X	X
Isopropyl	60.11784	690	X		
Propyl	60.11784	719	X	X	X
Diethyl	74.14784	704.8	X	X	X
N-dimethyl-ethyl	74.14784	675	X		
Isobutyl	74.14784	736	X		
Sec-butyl	74.14784	724	X		
Butyl	74.14784	740	X	X	X
Triethyl	102.19784	726	X	X	X
2-ethyl-N-butyl	102.19784	778	X		
N-ethyl-2-methyl-2-propan	102.19784	691	X		
Dipropyl	102.19784	757	X	X	
Tripropyl	144.27784	753	X	X	
N-methyl-dibutyl	144.27784	745	X		
Nonyl	144.27784	782	X	X	
Dipentyl	158.304	770	X		
Dihexyl	186.35784	795	X	X	
Tributyl	186.35784	778	X	X	
Triisobutyl	186.35784	766	X		

effects. The mobility was obtained under different temperature ($T = 14\,^{\circ}\text{C}$, 24 $^{\circ}\text{C}$, 34 $^{\circ}\text{C}$ and 41 $^{\circ}\text{C}$) and relative humidity (RH = 0 %, 20 % and 40 % at each temperature) conditions. For verification, we also repeated some measurements on a Structures for Lossless Ion Manipulation (SLIM)-based ion mobility spectrometer coupled with a ToF MS at the University of Tartu (UT). The measured mobilities were then used to probe and parameterise the drag enhancement factor (ξ), the effective gas–molecule collision diameter (d_g) and the polarisation correction to the Mason–Schamp's first approximation of the low-field kinetic theory using Kihara's extension of the Chapman–Enskog expansion in the free-molecular regime (Mason & Schamp, 1958).

2.1. Experiments

Alkylammonium salt samples ($10\,\mu\text{M}-1$ mM) were prepared using hydrochloric acid, sulphuric acid, and nitric acid from amines in methanol-water (50%v/v) solution. Samples with hydrochloric acid were used at IUPUI and with sulphuric acid and nitric acid at UHel. The cations were generated by electrospraying dilute salt solutions into the DMA using a pressurised silica capillary. Table 1 shows the 21 alkylammonium cations studied in this work, among which 12 were measured at both IUPUI and UHel, and 5 were repeated at UT using chemical ionisation with SLIM.

2.1.1. DMA-MS

At both IUPUI and UHel, the mobility measurement was performed using the commercial SEADM planar DMA (Amo-Gonzalez & Perez, 2018). A QStarXL was hyphenated to the DMA at IUPUI and was used to characterise the mass of the ions. The DMA–MS setup is a replicate of the one described by Rus, Moro et al. (2010). A similar setup was used at UHel, except the mass spectrometer was replaced by a Tofwerk ToF MS (Bianco et al., 2022).

As shown in Fig. 1a, sample solutions were introduced by electrospray ionisation (ESI) into a planar DMA, where a uniform electric field was applied between two parallel plate electrodes. By varying the high voltage applied on the front panel, analyte ions were selected based on their electric mobilities and directed to a mass spectrometer. The planar DMA was operated under atmospheric pressure in a closed sheath flow loop. We added a humidifier and a heat exchanger in the sheath loop to vary T and RH in mobility measurements. RH is controlled by changing both the water temperature (set by a hot plate) and the flow rate through the humidifier. At UHel, a cooling and heating bath thermostat (Lauda edition 2000) was used to control the sheath T, whereas at IUPUI, it was controlled by a chiller (ThermoCUBE 200–500) and heating tapes. A DHT22 sensor (accuracy: ± 2 % RH, ± 0.5 °C) mounted in the sheath loop was used to monitor T and RH. In this study, mobility measurements were conducted at T of 24 °C, 34 °C and 41 °C, and RH of 0% 20% and 40 % at both IUPUI and UHel. At UHel, a set of experiments was additionally performed at 14 °C. At IUPUI, zero air from Parker Balston SOURCE LCMS-5000 TriGas Generator was used, and at UHel, it was delivered from synthetic air cylinder (purity

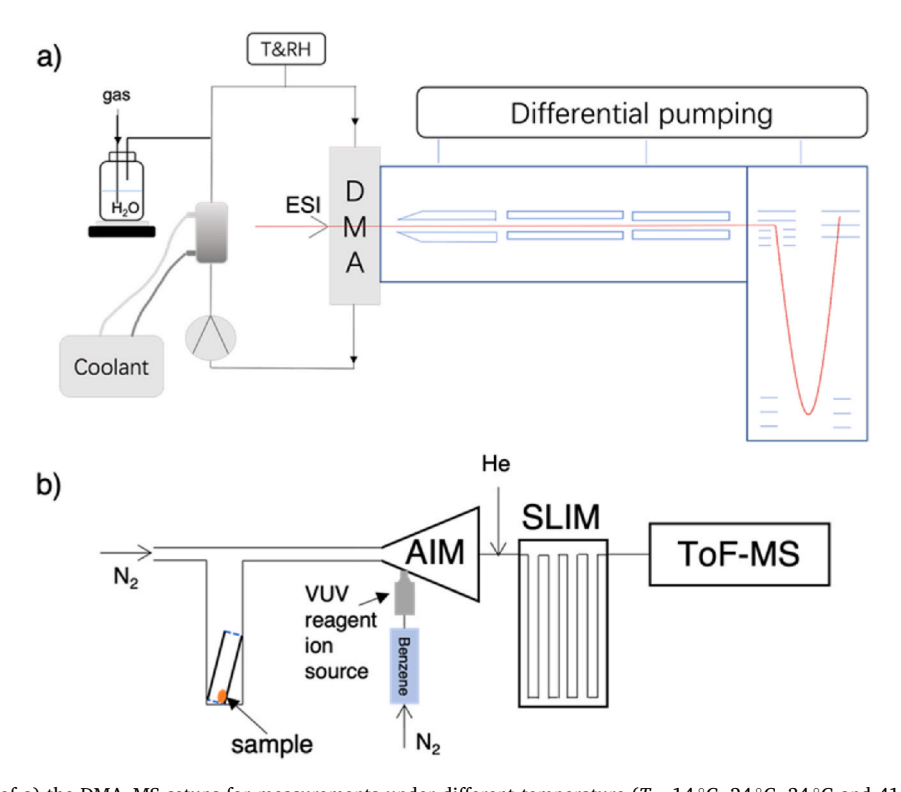


Fig. 1. Schematics of a) the DMA–MS setups for measurements under different temperature ($T=14\,^{\circ}\text{C}$, $24\,^{\circ}\text{C}$, $34\,^{\circ}\text{C}$ and $41\,^{\circ}\text{C}$) and relative humidity (RH = 0 %, 20 % and 40 %) conditions. b) the SLIM-MS setup using benzene cations as the reagent ion.

 \geq 99.999 %). We did calibrant measurements also in nitrogen (N₂) at UHel, where the gas was supplied from a liquid nitrogen container (purity grade 5.0).

Tetrabutylammonium cation was used as the mobility standard and was introduced to each sample, so that it was electrosprayed together with the analyte in each measurement cycle for internal calibration to minimise instrumental uncertainties. Knowing the mobility of the calibrant (K_{ref}) and the measured voltages for calibrant (V_{ref}) and analyte (V_a), the mobility of the analyte ion (K_a) can be obtained via

$$K_a = \frac{K_{\rm ref} V_{\rm ref}}{V_a} \ . \tag{1}$$

2.1.2. SLIM-MS

A Tofwerk SLIM-based ion mobility spectrometer coupled with a ToF MS (Vocus CI-IMS-TOF) was used in our study to verify the relative mobility of 5 analytes. In contrast to the uniform electric field applied in the DMA, the SLIM-based ion mobility spectrometer employs both direct current (DC) and radio frequency (RF) in creating the confining electric field and travelling wave to propel ions through the traversing path (Ibrahim et al., 2017). SLIM-based ion mobility spectrometers are operated in lower pressures than ambient (\sim 380 Pa). We used Tofwerk's AIM reactor to ionise amines directly using benzene cations produced by photoionisation (Fig. 1b). 1 μ L of amines was prepared in small pieces of 6 mm Teflon tube with both ends capped as sample permeation sources. A sample permeation source tube was placed in a 12 mm tube with one end sealed and the other end attached to a Tee-connector, where the analyte was allowed to diffuse into the nitrogen flow fed into the inlet of the AIM reactor. Helium was introduced after the AIM reactor into SLIM as the drift gas for mobility measurement.

2.2. Mobility-mass relation

In the free molecular regime for low fields, the ion mobility (K) is related to the inverse of the collision integral (Ω) which is also known as the collision cross section (CCS). This relationship is mass (m) dependent. Mason–Schamp's first approximation describes the relation as follows (Mason & Schamp, 1958; Revercomb & Mason, 1975)

$$K_{\rm MS} = \frac{3}{16} \frac{q}{N} \left(\frac{1}{m} + \frac{1}{m_{\rm g}} \right)^{1/2} \left(\frac{2\pi}{kT} \right)^{1/2} \frac{1}{\Omega},\tag{2}$$

where q=ze stands for the ionic charge with z being the number of charges and e the elementary charge, N is the number density of the drift gas and is connected to pressure as p=NkT. k is the Boltzmann constant, T is the drift gas temperature, and m and m_g are the molecular weight of the ion and drift gas, respectively. Under spherical assumption for elastic and specular collisions, it is possible to deduce a size parameter from the CCS, namely the mobility equivalent diameter or simply mobility diameter for hard spheres, $d_{K,HS}=(4\Omega_{HS}/\pi)^{1/2}$. However, the hard sphere model is too ideal to account for the irregular shape of real analyte ions, potential interactions between the ion and gas molecules, and nature of the drift gas. By using a drag enhancement factor (ξ) to link the CCS to the sum of the effective gas—molecule collision diameter (d_g) and ion mass diameter, $d_m=(6m/(\pi\rho))^{1/3}$, with ρ being the ion density (Fernández-García & Fernández de la Mora, 2013; Ku & Fernández de la Mora, 2009), it is possible to relax some limitations of the hard-sphere model.

The Stokes–Millikan equation that relates electrical mobility (K_{SM}) to mobility diameter ($d_{K,SM}$) based on parameterisation from Millikan's oil experiments in the slip correction is widely used in describing aerosol particles:

$$K_{\rm SM} = \frac{q}{3\pi u dv_{\rm SM}} \left[1 + \operatorname{Kn} \left(a + b e^{-\frac{c}{\operatorname{Kn}}} \right) \right],\tag{3}$$

where μ is the gas viscosity and Kn is the Knudsen number. a,b,c are constants parameterised from Millikan's experiments, depending on the choice of constant ϕ that relates gas viscosity to the mean free path (λ). The drag enhancement factor can be derived from Millikan's experiments as $\xi_{\rm M}=9\phi/(2(a+b))$ (Fernández-García & Fernández de la Mora, 2013). By using a=1.165,b=0.483, and $\phi=0.491$ (with a repulsive force between molecules) from Kim, Mulholland et al. (2005) as suggested in ISO15900, $\xi_{\rm M}=1.3407$. Larriba and Hogan (2013) reasoned the value of $\xi=1.3578$ when comparing Mason–Schamp with Stokes–Millikan by using a=1.257 and b=0.4 from Davies (1945) and $\phi=1$. Fernández-García and Fernández de la Mora (2013) got a slightly different value $\xi_{\rm M}=1.3552$ with $\phi=0.499$ (without a repulsive force between molecules). With this set of parameters, Ku and Fernández de la Mora (2009) found agreement between eqs. (2) and (3) when $d_{\rm g}=0.3$ nm for spheres. Therefore, it is possible to connect mobility diameter to mass diameter and CCS via

$$\Omega_{\rm o} = \frac{\pi}{4} \xi (d_{\rm m} + d_{\rm g})^2 = \frac{\pi}{4} d_{\rm K}^2 \tag{4}$$

and write the modified Mason-Schamp equation for spheres as

$$K = K_{\text{MS}} \cdot f(\xi, d_{\text{g}}) = \frac{3}{16} \frac{q}{N} \left(\frac{1}{m} + \frac{1}{m_{\text{g}}} \right)^{\frac{1}{2}} \left(\frac{2\pi}{kT} \right)^{\frac{1}{2}} \frac{1}{\Omega_{\text{o}}} \quad \text{with } f(\xi, d_{\text{g}}) = \frac{4\Omega}{\pi \xi (d_{\text{m}} + d_{\text{g}})^{2}}.$$
 (5)

Eq. (5) is valid when $Kn = 2\lambda/(d+d_g) \gg 1$ and is sometimes referred to as the *modified Stokes–Millikan law* (Fernández-García & Fernández de la Mora, 2013).

2.3. Mobility measurement calibration

We used tetrabutylammonium cation (TBA $^+$, m/z = 242.2842) as the mobility calibrant. Calibrant measurements were performed in both air and nitrogen and under different T (24 °C, 34 °C and 41 °C) and RH (0 %, 20 %, 40 %) conditions by maintaining the same instrumental conditions (e.g., blower speed, ESI voltage and distance of needle tip to DMA inlet). Since the DMA geometry remains the same, eq. (1) is valid to link measurements done in air and nitrogen and under different T and RH conditions.

The literature values for mobility standards are typically reported in CCS. The reported CCS value for TBA⁺ measured in nitrogen (N₂) is 167.5 Å² (Picache et al., 2019), which can be converted to mobility using eq. (2). The reduced mobility (K_0) equation can be used to link ion mobilities at different temperatures in dry conditions:

$$K_0 = K_1 \frac{P}{760} \frac{273.16}{T_1} = K_2 \frac{P}{760} \frac{273.16}{T_2} \Longrightarrow \frac{K_1}{K_2} = \frac{T_1}{T_2}$$
 (6)

To obtain the calibrant mobilities under humid conditions, we invoked the relation described in eq. (1) to link dry and humid measurements, $K_{0\%}V_{0\%} = K_{RH}V_{RH}$. By using eqs. (1) and (6), we can get a matrix of analyte mobilities under different T and RH in N₂. By applying eq. (1) again to measurements done at different drift gases, a matrix of TBA⁺ mobilities under different T and RH in air can be achieved, $K_{air} = K_{N_2}V_{N_2}/V_{air}$.

Calibrant measurements were missing at 14 °C in N_2 . To deduce TBA⁺ mobilities at 14 °C in air ($K_{14,RH,air}$), we took the average of the calculated TBA⁺ mobility at 14 °C in nitrogen scaled by the ratio between K_{air} and K_{N_2} under different T and RH conditions. Measured TBA⁺ mobilities at different temperatures suggested a linear T dependence for fixed RH. Based on the assumption that the linear dependence is extendable to 14 °C, it is possible to approximate $K_{14,RH,air}$ as follows

$$K_{14,0,\text{air}} = K_{14,0,N_2} \cdot \langle K_{\text{air}}/K_{N_2} \rangle_{\text{average}}$$

$$f = \frac{K_{14,0,\text{air}}}{(2K_{24,0,\text{air}} - K_{34,0,\text{air}})} \Longrightarrow K_{14,\text{RH,air}} = (2K_{24,\text{RH,air}} - K_{34,\text{RH,air}}) \cdot f.$$
(7)

3. Results

3.1. T, RH, and ion conformation effects

The ion mobilities measured using the two individual DMA–MS setups (i.e., UHel and IUPUI with scheme displayed in Fig. 2) are in excellent agreement (see Fig. 2c) under different T (24 °C, 34 °C and 41 °C) and RH (0 %, 20 %, 40 %) conditions. Both datasets are calibrated against the calibration data matrix displayed in Fig. 2a. Our mobility measurements under different T and RH show that ion mobility increases with increasing T and decreasing RH (Fig. 2a and b).

The measured mobilities were compared with computational modelling results. The molecular configurations for the studied ions were obtained via configurational sampling as described in detail in the Supporting Information. We computed ion mobilities using the Lennard-Jones 4-6-12 potential (parameters for nitrogen) with a quadrupole potential (TMLJqpol) using the IMoS program. The calculated mobilities are the Boltzmann averaged values over the found minimum energy structures (See Supplement S1). To study the humidity effect, we also modelled the mobilities of ion clusters with 1–3 water molecules. For comparison, ion mobilities were also calculated using the Trajectory Diffuse Hard Sphere Scattering (TDHSS) model with air parameterisations. TDHSS calculates ion mobility from the averaged drag force over a control volume that travels with the same velocity as the ion by assuming equal

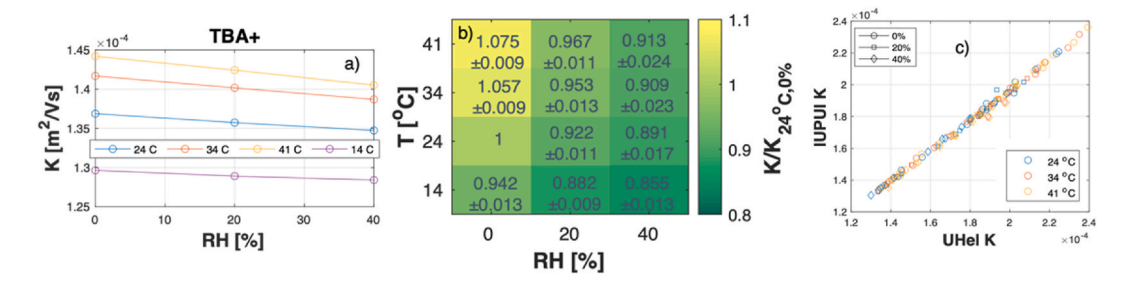


Fig. 2. a) Electrical mobility (K) of tetrabutylammonium cation (TBA $^+$) under different temperature (T = 14 °C, 24 °C, 34 °C and 41 °C) and relative humidity (RH = 0 %, 20 % and 40 %) conditions. b) Influences of temperature and relative humidity on ion mobility. Colour indicates mobility ratio with respect to mobility at 24 °C and 0 % humidity. The mean and standard deviation of mobility ratio (over 21 alkylammonium cations) are displayed for each temperature and relative humidity condition. c) Comparison of ion mobility (12 alkylammonium cations) measured at UHel and IUPUI under different temperature and relative humidity. (For interpretation of the references to colour in this figure legend, the reader is referred to the Web version of this article.)

probability for all positions in the free-molecular regime (Shrivastav et al., 2017). The TDHSS model employs a 4–∞ potential that accounts for ion-induced dipole interaction, it is known to often perform poorly for small ions when compared to the trajectory method using the Lennard-Jones potential. We used full accommodation and re-emission velocity from a distribution at 92 % of the energy of a Maxwell distribution in the calculations. The unsubstituted hydrogens on the ammonium nitrogen can to some extent relax steric strain in the protonated primary, secondary and tertiary alkylamines, which reduces the probability of these ions undergoing elastic collisions. Thus, the use of TDHSS with full accommodation gives extreme estimates of limiting conditions without the consideration of van der Waals interactions. The tabulated measured and calculated data are enclosed in Supplement S2.

The overall comparisons are shown in Figs. S1–2. Coincidentally, the TDHSS model gives good estimates, especially of dry mobilities at 14 °C for the smallest ions. This method tends to underestimate ion mobilities as *T*, RH, and/or ion mass change, giving errors of up to 25 %. One explanation for the discrepancy between the model and the experiments is that in the humid experiments the clusters are hydrated in the presence of water. Hence the hydrate distribution could explain why the model sometimes overestimates the mobility compared to experiments in humid conditions. For instance, the modelled mobility of dimethylammonium ion hydrated by one water molecule is lower than that of the bare monomer ion. Literature works have also proven the inappropriateness of applying this method to small ions (Larriba-Andaluz et al., 2015). The reason is simple. As the molecule gets smaller, the likelihood of a diffuse collision with the gas is reduced and collisions become more specular. In addition, we observed that the TDHSS model tends to underestimate mobilities of ions as mass increases in dry conditions.

The TMLJqpol on the contrary overestimates ion mobilities, especially for small masses (Fig. S2) where the discrepancy is up to 30% in the dry condition. The smallest differences between calculations and measurements are found in the larger tertiary alkylammonium ions and the calculated mobilities of primary alkylammonium ions have the largest deviations from the experimental values. Using nitrogen Lennard-Jones parameters in the mobility calculation possibly leads to slightly higher values, yet this cannot fully explain the large differences in dry conditions. The disagreement between measurements and calculations might either be attributed to solvation of ions in measurements or to missing interactions in mobility calculation. The recorded mass spectra hardly showed any traces of water clusters in dry conditions. Instead, we observed m/z peaks with a positive mass shift of 32 ($[M+32]^+$). This $[M+32]^+$ peak had the peculiarity of coinciding with the monomer ion $[M]^+$ peak in the mobility space, especially for the small primary alkylammonium ions (Fig. S 3a-b). Having the same mobility as the monomer ion peak suggests that both ions had the same structure through the whole mobility cell, and hence both probably come from direct derivatives of the bare monomer ion, including methanol solvation, oxygen clustering, or other ESI reactions. Comparison with TMLJqpol results suggests that the smallest ions could be clustered with 1–3 methanol molecules (Supplement S2), if the methanol solvation were the sole cause. Mass spectral analysis suggests a higher probability of methanol adduct than O_2 (Fig. S 3c). However, the effect of the latter candidate cannot be ruled out, because $[M+O_2]^+$ and $[M+Methanol]^+$ are contained in a single peak in the mass domain.

We used methanol-water (50% v/v) as the solvent and therefore there are more water than methanol molecules in the sample solution. Water and methanol form hydrogen bonding with comparable binding strength (Table S 1) and water is a smaller molecule. If the $[M+32]^+$ peak in dry conditions is due to methanol solvation, it remains unclear why there are hardly any water clusters in the mass spectra. Karpas (1989) reported mobilities of several different protonated aliphatic amines measured at 200 °C under atmospheric pressure, where a radioactive source was used for ionisation and amines were taken from the headspace vapours of commercially available samples. A temperature dependence was observed and Karpas, Berant et al. (1989) suggested that clustering with drift gas molecules was the cause of the reduction in mobility with temperature decrease. By taking into account the temperature effect on gas molecule clustering, our measured mobilities are close to the values reported in Karpas' works (Karpas, 1989, Karpas, Berant et al., 1989). In our measurements in dry air, we saw the $[M+32]^+$ peak usually emerges at the same voltage as the monomer ion. The coincidence is also occasionally observed with $[M+28]^+$. This can be ascribed to the fact that a mass shift of 28 may also result from a $(CH_2)_2$ group that could originate from longer-chained amine impurities in solution. Also, O_2 has a larger dipole polarisability than N_2 (Spelsberg & Meyer, 1994) and is more reactive, which could give it a better chance to end up with the ion in the mass detector.

We also performed a few experiments using ethanol and water as the solvent in dry N_2 , and in these cases $[M+28]^+$ was observed, but hardly any $[M+32]^+$. However, these tests were likely influenced by contaminants present in the measurement system, which limits the information that can be reliably extracted from them. Nonetheless, these analyses indicate that the large discrepancy between the measured and TMLJqpol mobilities in dry conditions most likely results from adduct formation on the monomer ions. Both methanol and O_2 (and occasionally N_2 or perhaps alkyl chain elongation) are possible candidates for the adduct. Adduct formation via clustering (or reactions) seems to be a common phenomenon associated with light ions under atmospheric pressures, which needs to be taken into consideration in the comparison of measurements with calculations.

In humid conditions, the methanol solvation was hardly observed and the $[M + H_2O]^+$ peak was of high intensity. The decrease of mobility with water loading we observed is in line with earlier studies on vapour uptake (Oberreit et al., 2015; Thomas et al., 2016; Li & Hogan, 2017, Ahonen et al., 2019). Compared with the TMLJqpol results, the smallest ions were clustered with ≥ 3 water molecules already at 20% RH (Fig. S 2); yet, TDHSS indicates 0–1 water molecule at both 20% and 40% RH (Fig. S1). As aforementioned, since the adduct identity especially in dry conditions and the number of water molecules in humid experiments are unknown, the calculation methods can only serve as an approximation to the number of possible adduct molecules present and are therefore only indicative.

Although the comparison between measured and calculated mobilities often correctly predicts the trends with respect to ion size, we must outline three pairs of ions (ethylammonium⁺ vs. trimethylammonium⁺, propylammonium⁺ vs. diethylammonium⁺, butylammonium⁺ vs. triethylammonium⁺), where the theoretical models predict the opposite trend from the measurements (Fig. S1 and Fig. 3a). The measured trend also violates the general relation of ion mobility to mass that ion mobility decreases with increasing

mass; yet it is seen in both the IUPUI and UHel datasets in air and in nitrogen. As suggested by the preceding analysis, the unexpected trends could result from adduct formation, possibly by clustering of solvent or drift gas.

To test the clustering hypothesis, we conducted measurements of diethylammonium⁺, butylammonium⁺, trimethylammonium⁺, propylammonium⁺, and triethylammonium⁺ using a SLIM-based IMS, where a similar trend to the calculation (TDHSS method) is observed (Fig. 3b–d). As SLIM measurements were performed using helium as the drift gas at about 380 Pa, the low pressure used in SLIM would significantly reduce the clustering probability around the ion. Also, the application of confining DC and RF in SLIM together with travelling wave can cause dielectric heating of the ion, which could possibly shorten the interaction time of the ion with gas molecules and further help to overcome the intermolecular binding energies. Karpas, Berant et al. (1989) observed that ion mobility measurements conducted in helium under atmospheric pressure demonstrated no gas clustering effect. Consequently, unlike the measurements performed under atmospheric pressure using the DMA, the SLIM arrival sequence aligns with the IMoS results that are based on the free-molecular theory.

Although the unexpected trends observed under atmospheric pressure in DMA–MS measurements are possibly affected by adduct formation, the larger mobilities for branched ions compared to their linear isomers (also seen in IMoS results) or to the smaller linear structures with one less CH_2 indicates the importance of ion structures in mobility determination. Typically, branched structures exhibit stronger steric effects than linear structures and are therefore less prone to clustering or reactions.

A clear mass dependence of the measured ion mobility can be observed (Fig. 4) when separating the data according to ion structures into linear (primary alkylammonium cations with a linear alkyl chain), di-branched (secondary alkylammonium cations with identical alkyl chains) and tri-branched (tertiary alkylammonium cations with identical alkyl chains) groups. Ion mobility decreases slightly more rapidly with mass increase in the linear group than for the branched ions. When adding water into the drift gas, the *T* effect attenuates while ions become more and more separated by structure groups, which may suggest that water can potentially be used as a dopant in probing ion structural information in mobility studies.

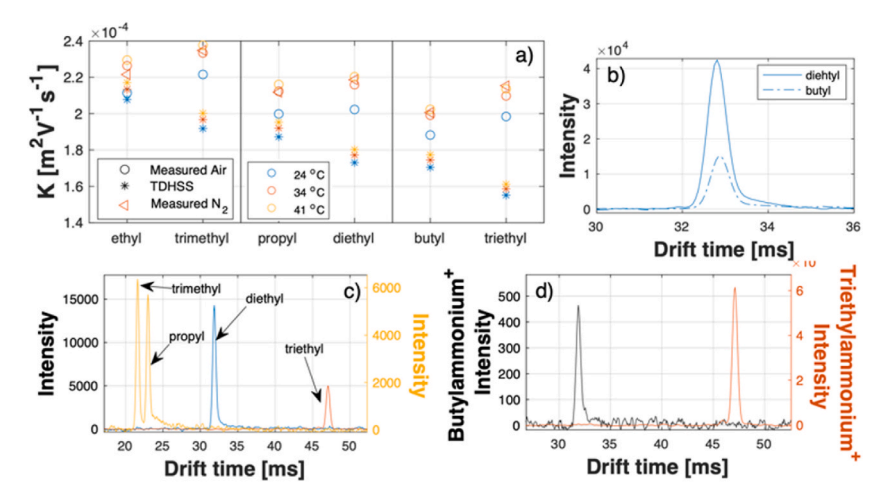


Fig. 3. a) Discrepancy between measured mobility using planar DMA and calculation using $4-\infty$ potential in the trajectory method (TDHSS) with full accommodation and re-emission velocity from a distribution at 92 % of the energy of a Maxwell distribution in IMoS. b–d) Drift time of diethylammonium⁺, butylammonium⁺, trimethylammonium⁺, propylammonium⁺, and triethylammonium⁺ measured by SLIM-based IMS in nitrogen.

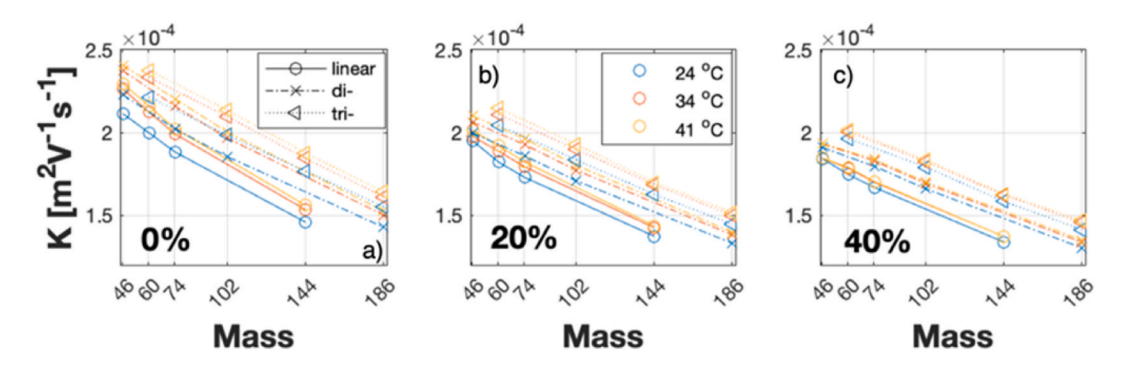


Fig. 4. Ion mobility dependency on mass and ion structure. Different markers indicate different ion structures: linear (primary alkylammonium cations with a linear alkyl chain, 'o'), di-branched (secondary alkylammonium cations with identical alkyl chains, ' \times ') and tri-branched (tertiary alkylammonium cations with identical alkyl chains, ' \wedge ') groups.

3.2. Drag enhancement factor (ξ) and effective gas-molecule collision diameter (d_g)

Although our analyte ions are not of spherical shape, if we assume the measured mobilities are equivalent mobilities for spheres, it is possible to probe the sensitivity of the drag enhancement factor (ξ) and effective gas-molecule collision diameter ($d_{\rm g}$) with respect to ion structures using eq. (5). By fitting the structure-separated data in each T and RH combined condition, we obtain ξ in the range of 1.30–1.39 and $d_{\rm g}$ in the range of 0.26–0.43 nm. Three fitted ξ values are smaller than 1.34, paired with $d_{\rm g}\approx 0.26$ nm, found for tribranched structures in dry conditions. The coefficient of determination (R^2) measure of goodness-of-fit (GoF) suggests that these fittings could explain 93–94 % of the data behaviour, which are the lowest among all the fits. The other GoFs are in the range of 97.2–99.7 %. The overall ξ is 1.359 ± 0.023 ($\xi=1.366\pm0.011$ by excluding $\xi<1.34$) and $d_{\rm g}$ is 0.32 ±0.051 nm ($d_{\rm g}=0.338\pm0.047$ nm by excluding $d_{\rm g}=0.338\pm0.047$ nm by e

Boxplots separated by structure, T and RH groups reveal weak non-linear dependences of ξ on structure and RH, but not on T (Fig. 5). ξ is found to be independent of the gas used in the mobility measurement and is related to the partition between specular and diffuse collisions (Epstein, 1924; Millikan, 1923). Although T could affect ξ through altering the interaction time of collisions, its influence is not expected to be obvious over 20 °C. While the collision nature may also vary with ion shape and RH, it is difficult to rationalise the non-linearity. d_g is observed to drop in more branched structures and as T increases. The dependence of d_g on structure may be influenced by the different steric strain of primary, secondary, and tertiary amines. Linear structures are more flexible compared to branched structures. As ions become more compact, the reduced random swing and vibration possibly allow collisions with gas molecules to happen at shorter distances on average, which may explain why $d_g = 0.28 \pm 0.017$ nm ($d_g = 0.29 \pm 0.0088$ nm by excluding d_g corresponding to $\xi < 1.34$) for tri-branched structures from our data approaches values reported in literature, 0.26 nm found by Fernández-García and Fernández de la Mora (2013) and 0.3 nm by Ku and Fernández de la Mora (2009). Gas molecules possess higher kinetic energy at higher T, possibly allowing them to approach slightly closer to the ion upon collision. We also observed RH rising effectively enlarging d_g . Water molecules can readily form hydrogen bonds with ions. The higher the RH, the more water molecules are available for the interaction, creating more resistance in the ion travelling path.

3.3. Correction to mason-schamp equation

Least-squares linear regression is used to parameterise T, RH, and ion structure effects on ξ and d_g . The quality of the fitted models is then examined by an ANOVA F-test. With each term in the models passing a F-test at 95% confidence interval, the optimised models for ξ and d_g are

$$\xi \sim 1.3276 - 0.00032579 \cdot RH + 0.065233 \cdot S + 0.00082159 \cdot RH \cdot S - 2.2312 \cdot 10^{-5} \cdot RH^2 - 0.023654 \cdot S^2$$

$$d_g \sim 0.74488 - 0.0011077 \cdot T + 0.0035224 \cdot RH - 0.074739 \cdot S - 0.0036107 \cdot RH \cdot S - 2.5094 \cdot 10^{-5} \cdot RH^2 + 0.0083446 \cdot S^2 + 1.0184 \cdot 10^{-5} \cdot T \cdot RH \cdot S.$$
(8)

S is the ion structure with S=1,2,3 for linear, di- and tri-structures. The ANOVA statistics also suggest that the temperature term in the linear model of ξ is insignificant at the 5 % significance level, hence we removed this term. The optimised models can explain about 84.2 % of the variability in ξ and 98.7% in $d_{\rm g}$. The response variables and the predicted ξ and $d_{\rm g}$ stay close to the 1:1 line, respectively

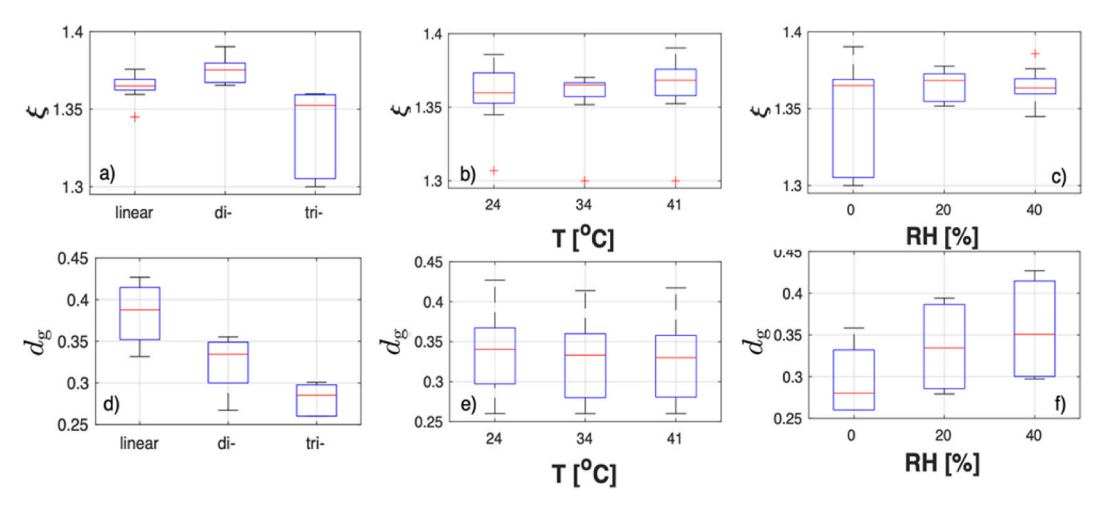


Fig. 5. The drag enhancement factor (ξ) and effective gas-molecule collision diameter ($d_{\rm g}$) derived from fitting modified Mason–Schamp equation ($K_{\rm MS} \cdot f(\xi, d_{\rm g})$) to the measured ion mobility (UHel setup). Data are separated by ion structure, temperature (T) and relative humidity (RH).

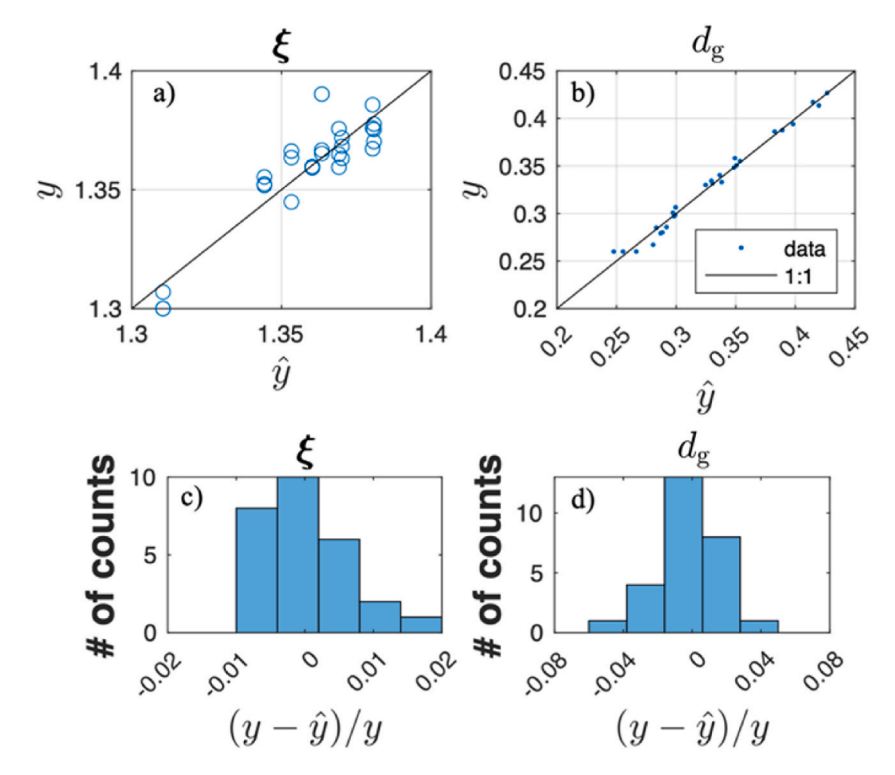


Fig. 6. a–b) The drag enhancement factor (ξ) and effective gas-molecule collision diameter (d_g) derived from fitting the modified Mason–Schamp equation $(K_{MS} \cdot f(\xi, d_g))$ to the measured ion mobility (UHel setup) vs. ξ and d_g values obtained using linear models composed of temperature, relative humidity and ion structural information. c–d) The respective residuals of the linear models of ξ and d_g presented as the ratio to the response variable, $(y - \hat{y})/y$.

(Fig. 6). The deviation is within ± 2 % for ξ and ± 6 % for d_g .

As an ion travels through the drift gas in the mobility measurements, it can polarise the surrounding gas molecules on its path. As a result, the interactions between an ion and neutral gas molecules are strongly affected by the polarisation effect. For mobility measurements in air at the temperatures studied there, polarisation dominates the ion-neutral interactions (Mason & McDaniel, 1988). According to Fernández-García and Fernández de la Mora (2013), the polarisation effect may be accounted for by a multiplier term to eq. (5) as a function of the normalised polarisation potential by thermal energy ($\varepsilon^* = \frac{2\alpha(q\varepsilon)^2}{\pi\varepsilon_0kT(d+d_g)^4}$, where α is the gas-molecule

polarisability and ε_0 is the permittivity of vacuum). For air, $\alpha=1.7~\text{Å}^3$. The polarisation parameter ε^* is dimensionless, which unlike the observations in Fernández-García and Fernández de la Mora (2013) is not linearly related to the ratio between our measured mobilities and the calculated values using eq. (5) and the parameterisations in eq. (8) (shown in Fig. 6a). Larriba and Hogan (2013) suggested the approach $\Omega=\mathcal{L}\xi PA$ where \mathcal{L} is a complex non-linear correction factor for polarisation, and a function of ε^* (labelled as φ_e in their work) and ξ :

$$\begin{split} \mathcal{L} \sim \left[1 + \varphi_e \left(\frac{1}{3.1} + \frac{1}{\xi} \left(\frac{1}{16} + \frac{4}{33} \varphi_e\right)\right)\right] if \ \varphi_e \leq 1 \\ \\ \mathcal{L} \sim \left[1 + \varphi_e \left(\frac{1}{4} - \frac{2.3}{1000} \varphi_e + \frac{1}{\xi} \left(\frac{9}{56} - \frac{6.8}{1000} \varphi_e\right)\right)\right] if \ \varphi_e > 1 \end{split}$$

These equations were based on using IMoS to calculate the effect of polarisation on a sphere separating direct momentum impinging and grazing collisions and are not derived from experimental observations.

Here, we used a Gaussian function to depict the bell shape and skewed it using a power function for fitting to the experimental data. The polarisation correction term therefore takes the following form:

$$f(\varepsilon^*) = \frac{c}{a \cdot \sqrt{2 \cdot \pi}} \cdot e^{-\frac{\left(\varepsilon^* - b\right)^2}{2 \cdot a^2}} + d,\tag{9}$$

where a, b, c, d and h are coefficients. d is a scaling factor chosen as a constant, d = 0.6, in our treatment. Eq. (9) captures the variation of $\frac{K}{K_{MS} \cdot f(\xi, d_e)}$ with ε^* well and is able to explain over 99 % of the variability in most cases (Fig. 7).

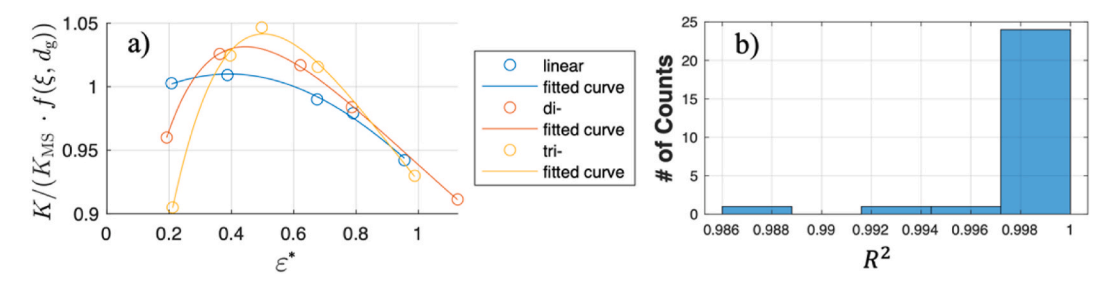


Fig. 7. a) The ratio between measured and theoretical mobilities based on the modified Mason–Schamp equation $(K/(K_{\rm MS} \cdot f(\xi, d_g)))$ vs. the polarisation parameter (ε^*) with fitted curves using the modified gaussian distribution. b) Distribution of goodness of fit (GoF) R^2 of fittings to data separated by structure, T and RH using eq. (9).

Fitting eq. (9) to structure, T and RH separated data allows us to determine the connections of the coefficients to ion structures, T and RH. We consulted least squares linear regression and performed a F-test on each regression term and found that the following models can best describe a/c, a, $b^{1/h}$ and b in eq. (9):

$$\frac{a}{c} \sim 0.96315 - 5.9315 \cdot 10^{-6} \cdot T \cdot RH - 7.6751 \cdot 10^{-5} \cdot T \cdot S + 0.00095043 \cdot RH \cdot S$$

$$a \sim 1.7197 - 1.0924 \cdot S - 0.00019824 \cdot T \cdot RH + 0.057663 \cdot RH \cdot S + 0.00062036 \cdot T \cdot S^{2} - 0.011952 \cdot RH \cdot S^{2}$$

$$b^{\frac{1}{h}} \sim 0.37597 + 0.012228 \cdot RH + 0.044693 \cdot S - 5.0513 \cdot 10^{-5} \cdot T \cdot RH$$

$$h \sim 1.5711 - 0.94335 \cdot S - 0.00024211 \cdot T \cdot RH + 0.078351 \cdot RH \cdot S + 0.15924 \cdot S^{2} - 0.017166 \cdot RH \cdot S^{2}$$
(10)

These models can explain 45.9 %, 80 %, 92.8 % and 78.8 % of a/c, a, $b^{1/h}$ and h, respectively (Fig. 8). Except for a/c, the rest of the coefficients in eq. (9) that govern the width, the location of the maximum and the skewness of the curve shape can be relatively well predicted using ion structures, T and RH.

The calculated polarisation correction using eq. (9) and the models of coefficients in eq. (10) is comparable to the ratio between

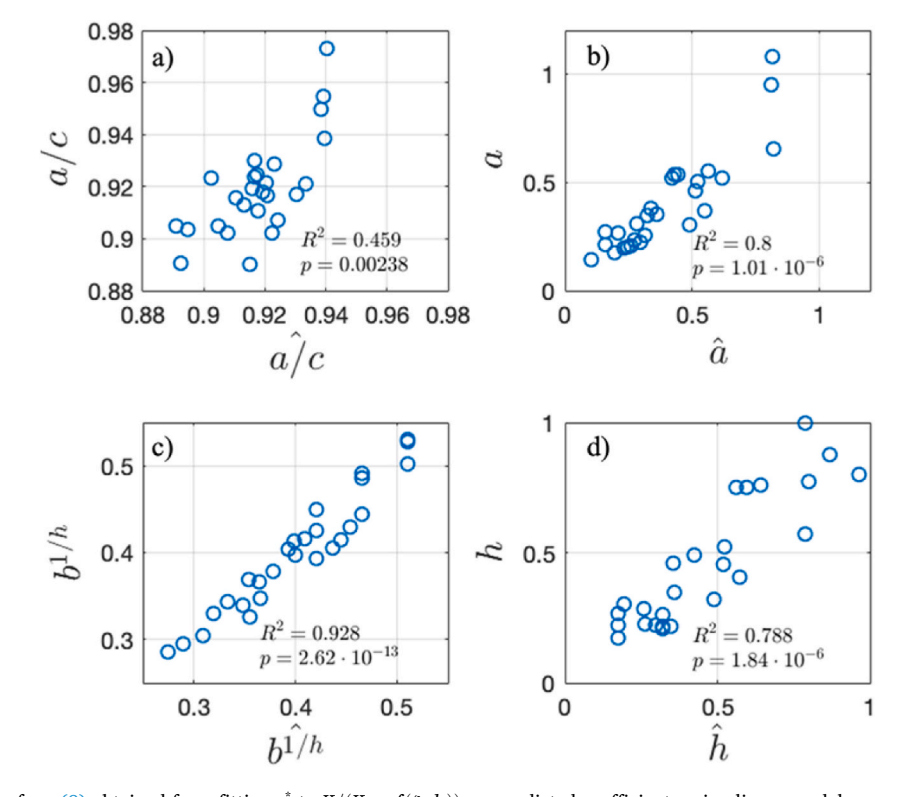


Fig. 8. Coefficients of eq. (9) obtained from fitting ε^* to $K/(K_{\rm MS} \cdot f(\xi, d_g))$ vs. predicted coefficients using linear models composed of temperature, relative humidity and ion structural information. Coefficient of determination (R^2) and p-value for the F-test on the model are given for each coefficient.

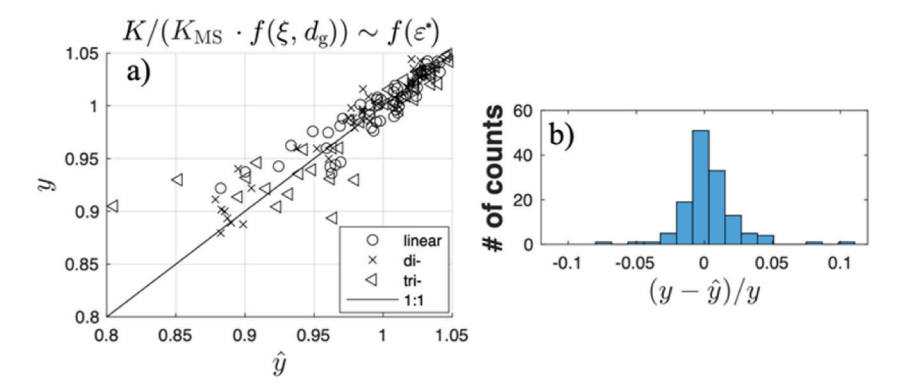


Fig. 9. a) $K/(K_{MS} \cdot f(\xi, d_g))$ vs. modelled polarisation correction $f(\varepsilon^*)$ using coefficients predicted by linear models using temperature, relative humidity, and ion structural information. b) Model residuals presented as the ratio of the difference between the response variable (y) and the prediction (\widehat{y}) to the response variable, $(y-\widehat{y})/y$.

measured and calculated mobilities using eq (5) and ξ and d_g parameterisations in eq. (8) (see Fig. 9). The discrepancy is within $\pm 10\%$.

3.4. Model validation

We applied eq. (5) with the polarisation correction described in eq. (9) using parameterisations of ξ , d_g , a/c, a, $b^{1/h}$ and b from this work to predict the mobilities of the 9 other alkyl ammonium cations measured only at IUPUI (see Fig. 10). Except for dipentylammonium⁺, these alkylammonium cations contain branches of unidentical functional groups. The predicted mobilities for dipentylammonium⁺

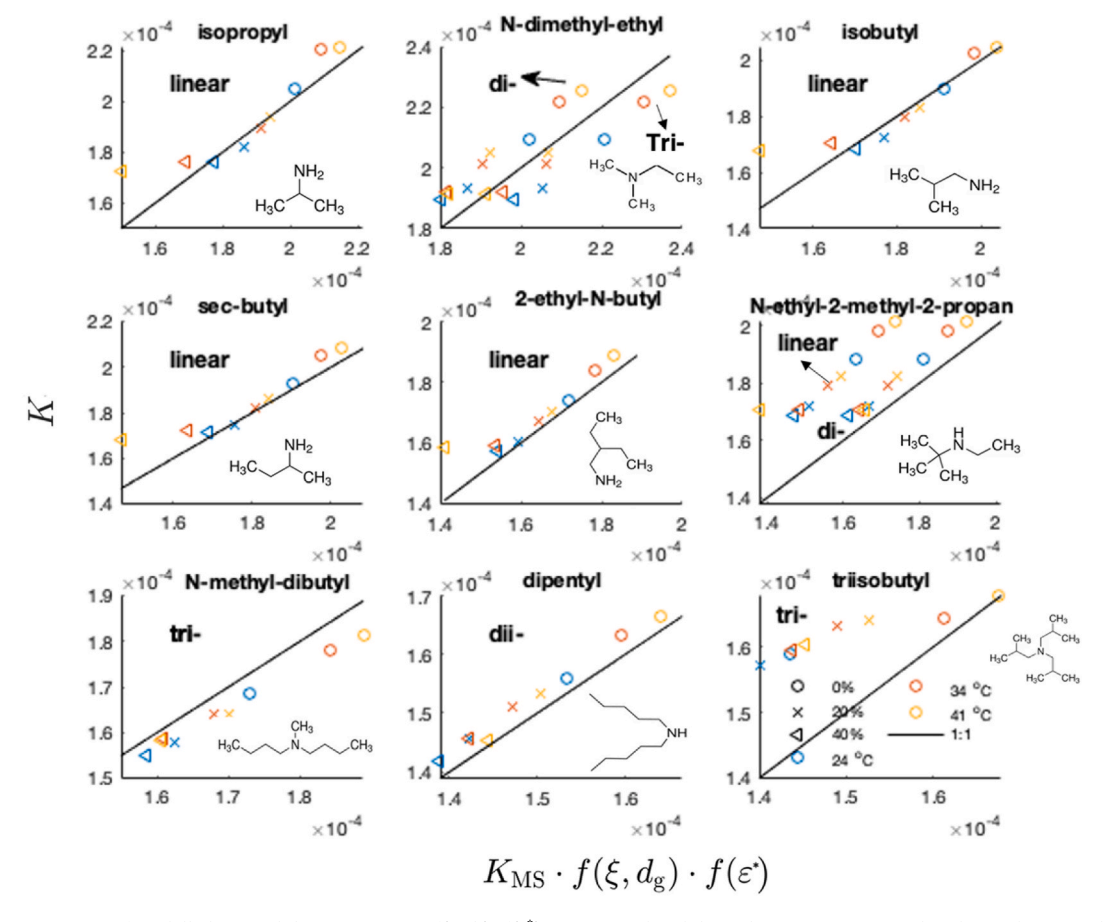


Fig. 10. Comparison of modelled ion mobilities using $K_{\text{MS}} \cdot f(\xi, d_{\text{g}}) \cdot f(\varepsilon^*)$ to measured mobility. The ion structure used in the prediction is displayed for each ion.

along the 1:1 line with the measured data but are slightly lower. The comparison between the measured and predicted mobilities indicate that isopropyl, isobutyl, sec-butyl, and 2-ethyl-N-butyl ammonium⁺ behave more like the linear type, though they also have some trace of the di-branched group. These ions are primary alkylammonium cations and have the general structure of H_3N^+R as in the linear case. N-ethyl-2-methyl-2-propanammonium⁺, which is a secondary alkylammonium cation, is closer to the di-branched type. The tertiary N-dimethyl-ethyl and N-methyl-dibutyl ammonium⁺, however, tend to have similarities to both di-and tri-branched structures, which may be attributed to unequal length of the alkyl chains in the tail. Our model significantly underestimates the mobility of triisobutylammonium⁺, likely because of the more compact conformation brought by the isobutyl groups in the tail.

4. Conclusions

We measured ion mobilities of alkylammonium cations in air under different temperature ($T=14\,^{\circ}$ C, $24\,^{\circ}$ C, $34\,^{\circ}$ C and $41\,^{\circ}$ C) and relative humidity (RH = 0 %, 20 %, 40 %) conditions. 12 analytes were measured using two individual planar DMA–MS setups and the results were in excellent agreement. In general, mobility increases with rising T and decreases with loading water vapour. In addition, the mobility dependence on mass is clearly observed when separating the measurement data by ion structural information. For several ions, we observed significant discrepancies between the measured and calculated ion mobilities, which is possibly caused by adduct formation on the monomer ions via clustering (or reactions). In dry conditions, both methanol and oxygen (occasionally nitrogen or alkyl chain elongation) are possible candidates of the adduct, and the mechanism behind the phenomenon requires further investigation. Adduct formation seems to be a common phenomenon associated with light ions under atmospheric pressures, and therefore taking it into consideration in performing simulations using density functional theory for mobility calculations brings insightful information in the interpretation of experimental data.

Karpas' works pointed at gas clustering possibilities (Karpas, 1989, Karpas, Berant et al., 1989). In atmospheric pressure measurements, the drift gas molecules constantly interact with the ion due to polarisation, which may seemingly result in gas molecules clustering around the ion as it travels, in particular at low temperatures. This may create a pressure-dependent 'continuum-like' effect that is not described by the free-molecular theory, which could be worth further exploration in theoretical mobility calculations.

The modified Mason–Schamp's approximation $(K_{\rm MS} \cdot f(\xi, d_{\rm g}))$ can be used to link measured mobility to mobility equivalent diameter for spheres via a drag enhancement factor ξ . The mobility equivalent diameter for spheres can be expressed as a sum of ion mass diameter $d_{\rm m}$ and an extra length from the effective gas-molecule collision diameter $d_{\rm g}$. Our data gave $\xi=1.359\pm0.023$ (1.366 ±0.011 by excluding $\xi<1.34$) and $d_{\rm g}=0.32\pm0.051$ nm (0.338 ±0.047 nm by excluding $d_{\rm g}$ corresponding to $\xi<1.34$) using $K_{\rm MS} \cdot f(\xi, d_{\rm g})$. We observed weak non-linear dependence of ξ only on ion structures and RH, but $d_{\rm g}$ values were well separated by structures and RH and slightly by T. $d_{\rm g}$ decreases with decreasing T and increasing number of branches in the ion structure and increases with rising RH.

Ions travelling through a neutral gas medium experience ion-induced dipole interactions with surrounding gas molecules. For air, the polarisation is the dominant contribution to the drag force. We followed the idea proposed by Fernández-García and Fernández de la Mora (2013) to parameterise the polarisation correction term from experimental data. However, our data exposed a non-linear dependence on the polarisation parameter ε^* . We found that the shape can be well captured using a modified Gaussian function with a power function. The coefficients in the modified Gaussian function as well as ξ and d_g were parameterised using linear models for ion structures, T, and RH. The mobilities calculated by the final model $K_{\rm MS} \cdot f(\xi, d_g) \cdot f(\varepsilon^*)$ using our parametrisations resulted in

± 10 % deviation from the measured data.

We further used 9 other alkylammonium cations for validation of the model. Only one of these 9 cations is of a di-branched structure. The rest have unidentical alkyl structures. Although in theory our model is not able to explain these ion structures correctly, it can help to reveal their similarity to linear, di- or tri-structures. Except for triisobutylammonium⁺, our model was able to predict the mobilities moderately well. The results indicate that the studied primary alkylammonium ions resemble the linear structures and the studied secondary ions behave like the di-branched structures, but the studied tertiary ions tend to possess the properties of both di- and tri-branched structures. The large discrepancy for triisobutylammonium⁺ likely comes from the more compact alkyl tail, which is not properly represented by the linear alkyl structures used in our parameterisation, implying that the polarisation effect is functional group dependent and related to ion chemical properties.

CRediT authorship contribution statement

Xuemeng Chen: Writing – review & editing, Writing – original draft, Visualization, Validation, Software, Resources, Project administration, Methodology, Investigation, Funding acquisition, Formal analysis, Data curation, Conceptualization. **Juha Kangasluoma:** Writing – review & editing, Resources, Funding acquisition. **Jakub Kubečka:** Writing – review & editing, Writing – original draft, Visualization, Software, Resources, Methodology, Investigation, Funding acquisition, Formal analysis, Data curation. **Ivo Neefjes:** Writing – review & editing, Writing – original draft, Visualization, Software, Methodology, Investigation, Formal analysis, Data curation. **Hanna Vehkamäki:** Writing – review & editing, Resources, Funding acquisition. **Markku Kulmala:** Resources, Funding acquisition. **Amirreza Tootchi:** Validation, Data curation. **Farah Mubas Sirah:** Validation, Data curation. **Leyan Hua:** Validation, Data curation. **Carlos Larriba-Andaluz:** Writing – review & editing, Writing – original draft, Supervision, Software, Resources, Project administration, Methodology, Investigation, Funding acquisition, Conceptualization. **Heikki Junninen:** Writing – review & editing, Resources, Project administration, Funding acquisition.

Declaration of competing interest

The authors declare that they have no known competing financial interests or personal relationships that could have appeared to influence the work reported in this paper.

Data availability

Data will be made available on request.

Acknowledgements

This project has received funding from the European Union's Horizon 2020 research and innovation programme under the Marie Skłodowska-Curie grant agreement No 896914. The authors also thank European Union (MSCA, HYDROCLUSTER, project 101105506), the Academy of Finland (Centers of Excellence Program, CoE VILMA, Grant No. 346368), the Research Council of Finland (346370, 325656,1356134), NSF grants No. 1904879 and 2203968, Estonian Research Council project PRG714 and Estonian Environmental Observatory (KKOBS project 2014-2020.4.01.20-0281) for financial support.

The numerical results presented in this work were obtained at the Centre for Scientific Computing, Aarhus http://phys.au.dk/forskning/cscaa/.

Funded by the European Union. Views and opinions expressed are however those of the author(s) only and do not necessarily reflect those of the European Union or the European Research Executive Agency. Neither the European Union nor the granting authority can be held responsible for them.

Appendix A. Supplementary data

Supplementary data to this article can be found online at https://doi.org/10.1016/j.jaerosci.2024.106353.

The authors gratefully appreciate the technical supports and help from Hannu Koskenvaara, Dr. Pekka Rantala, Dr. Runlong Cai, Dr. Pasi Aalto, Jarkko Mäntylä and Dr. Petri Keronen from the University of Helsinki; Viraj D. Gandhi, Xi Chen, Mohsen Latif, Leyan Hua and Kevin Carr from IUPUI; and Kalju Tamme, Aare Luts and Jaan Maasepp from the University of Tartu. X.C. would also like to thank Liina Kangur from the University of Tartu for providing diethylamine for the mobility analysis.

References

Ahonen, L., Li, C., Kubecka, J., Iyer, S., Vehkamaki, H., Petaja, T., Kulmala, M., & Hogan, C. J., Jr. (2019). Ion mobility-mass spectrometry of iodine pentoxide-iodic acid hybrid cluster anions in dry and humidified atmospheres. *Journal of Physical Chemistry Letters*, 10(8), 1935–1941.

Almeida, J., Schobesberger, S., Kurten, A., Ortega, I. K., Kupiainen-Maatta, O., Praplan, A. P., Adamov, A., Amorim, A., Bianchi, F., Breitenlechner, M., David, A., Dommen, J., Donahue, N. M., Downard, A., Dunne, E., Duplissy, J., Ehrhart, S., Flagan, R. C., Franchin, A., ... Kirkby, J. (2013). Molecular understanding of sulphuric acid-amine particle nucleation in the atmosphere. *Nature*, 502(7471), 359–363.

Amo-Gonzalez, M., & Perez, S. (2018). Planar differential mobility analyzer with a resolving power of 110. Analytical Chemistry, 90(11), 6735-6741.

Atkinson, R. W., Mills, I. C., Walton, H. A., & Anderson, H. R. (2015). Fine particle components and health–a systematic review and meta-analysis of epidemiological time series studies of daily mortality and hospital admissions. *Journal of Exposure Science and Environmental Epidemiology*, 25(2), 208–214.

Bianco, A., Neefjes, I., Alfaouri, D., Vehkamaki, H., Kurten, T., Ahonen, L., Passananti, M., & Kangasluoma, J. (2022). Separation of isomers using a differential mobility analyser (DMA): Comparison of experimental vs modelled ion mobility. *Talanta*, 243, Article 123339.

Campuzano, I., Bush, M. F., Robinson, C. V., Beaumont, C., Richardson, K., Kim, H., & Kim, H. I. (2012). Structural characterization of drug-like compounds by ion mobility mass spectrometry: Comparison of theoretical and experimentally derived nitrogen collision cross sections. *Analytical Chemistry*, 84(2), 1026–1033.
Curtius, J. (2006). Nucleation of atmospheric aerosol particles. *Comptes Rendus Physique*, 7(9–10), 1027–1045.

Davies, C. N. (1945). Definitive equations for the fluid resistance of spheres. Proceedings of the Physical Society, 57(4), 259-270.

Dodds, J. N., & Baker, E. S. (2019). Ion mobility spectrometry: Fundamental concepts, instrumentation, applications, and the road ahead. *Journal of the American Society for Mass Spectrometry*, 30(11), 2185–2195.

Dodds, J. N., May, J. C., & McLean, J. A. (2017). Investigation of the complete suite of the leucine and isoleucine isomers: Toward prediction of ion mobility separation capabilities. *Analytical Chemistry*, 89(1), 952–959.

Epstein, P. S. (1924). On the resistance experienced by spheres in their motion through gases. Physics Reviews, 23(6), 710-733.

Fernández-García, J., & Fernández de la Mora, J. (2013). Measuring the effect of ion-induced drift-gas polarization on the electrical mobilities of multiply-charged ionic liquid nanodrops in air. *Journal of the American Society for Mass Spectrometry*, 24(12), 1872–1889.

Gabelica, V., & Marklund, E. (2018). Fundamentals of ion mobility spectrometry. Current Opinion in Chemical Biology, 42, 51-59.

Ge, X., Wexler, A. S., & Clegg, S. L. (2011). Atmospheric amines - Part I. A review. Atmospheric Environment, 45(3), 524-546.

Ibrahim, Y. M., Hamid, A. M., Deng, L., Garimella, S. V., Webb, I. K., Baker, E. S., & Smith, R. D. (2017). New frontiers for mass spectrometry based upon structures for lossless ion manipulations. *The Analyst*, 142(7), 1010–1021.

Karpas, Z. (1989). Ion mobility spectrometry of aliphatic and aromatic amines. Analytical Chemistry, 61, 684-689.

Karpas, Z., Berant, Z., & Shahal, O. (1989). Effect of temperature on the mobility of ions. Journal of the American Chemical Society, 11, 6015-6018.

Kerminen, V. M., Chen, X., Vakkari, V., Petäjä, T., Kulmala, M., & Bianchi, F. (2018). Atmospheric new particle formation and growth: Review of field observations. Environmental Research Letters, 13, Article 103003.

Kieloaho, A.-J., Hellén, H., Hakola, H., Manninen, H. E., Nieminen, T., Kulmala, M., & Pihlatie, M. (2013). Gas-phase alkylamines in a boreal Scots pine forest air. Atmospheric Environment, 80, 369–377.

Kim, H., Kim, H. I., Johnson, P. V., Beegle, L. W., Beauchamp, J. L., Goddard, W. A., & Kanik, I. (2008). Experimental and theoretical investigation into the correlation between mass and ion mobility for choline and other ammonium cations in N2. *Analytical Chemistry*, 80, 1928–1936.

Kim, J., Mulholland, G. W., Kukuck, S. R., & Pui, D. Y. H. (2005). Slip correction measurements of certified PSL nanoparticles using a nanometer differential mobility analyzer (Nano-DMA) for knudsen number from 0.5 to 83. Journal of Research of the National Institute of Standards and Technology, 110(1), 31–54.

- Krechmer, J. E., Groessl, M., Zhang, X., Junninen, H., Massoli, P., Lambe, A. T., Kimmel, J. R., Cubison, M. J., Graf, S., Lin, Y.-H., Budisulistiorini, S. H., Zhang, H., Surratt, J. D., Knochenmuss, R., Jayne, J. T., Worsnop, D. R., Jimenez, J.-L., & Canagaratna, M. R. (2016). Ion mobility spectrometry–mass spectrometry (IMS–MS) for on- and offline analysis of atmospheric gas and aerosol species. Atmospheric Measurement Techniques, 9(7), 3245–3262.
- Ku, B. K., & Fernández de la Mora, J. (2009). Relation between electrical mobility, mass, and size for nanodrops 1–6.5 nm in diameter in air. Aerosol Science & Technology, 43(3), 241–249.
- Kulmala, M., Petaja, T., Ehn, M., Thornton, J., Sipila, M., Worsnop, D. R., & Kerminen, V. M. (2014). Chemistry of atmospheric nucleation: On the recent advances on precursor characterization and atmospheric cluster composition in connection with atmospheric new particle formation. *Annual Review of Physical Chemistry*, 65, 21–37
- Kulmala, M., Petaja, T., Nieminen, T., Sipila, M., Manninen, H. E., Lehtipalo, K., Maso, M. D., Aalto, P. P., Junninen, H., Paasonen, P., Riipinen, I., Lehtinen, K. E., Laaksonen, A., & Kerminen, V.-M. (2012). Measurement of the nucleation of atmospheric aerosol particles. *Nature Protocols*, 7(9), 1651–1667.
- Larriba, C., & Hogan, C. J. (2013). Ion mobilities in diatomic gases: Measurement versus prediction with non-specular scattering models. *The Journal of Physical Chemistry A*, 117(19), 3887–3901.
- Larriba-Andaluz, C., Fernandez-Garcia, J., Ewing, M. A., Hogan, C. J., Jr., & Clemmer, D. E. (2015). Gas molecule scattering & ion mobility measurements for organic macro-ions in He versus N2 environments. *Physical Chemistry Chemical Physics*, 17(22), 15019–15029.
- Lee, J. W., Lee, H. H. L., Davidson, K. L., Bush, M. F., & Kim, H. I. (2018). Structural characterization of small molecular ions by ion mobility mass spectrometry in nitrogen drift gas: Improving the accuracy of trajectory method calculations. *The Analyst*, 143(8), 1786–1796.
- Li, C., & Hogan, J. C. J. (2017). Vapor specific extents of uptake by nanometer scale charged particles. Aerosol Science and Technology, 51(5), 653-664.
- Mason, E. A., & McDaniel, E. W. (1988). Transport properties of ions in gases. New York, Chichester, Brisbane, Toronto, Singapore: John Wiley & Sons.
- Mason, E. A., & Schamp, H. W. (1958). Mobility of gaseous lons in weak electric fields. Annals of Physics, 4(3), 233-270.
- Millikan, R. A. (1923). The general law of fall of a small spherical body through a gas, and its bearing upon the nature of molecular reflection from surfaces. *Physics Reviews*, 22(1), 1–23.
- Mirme, S., & Mirme, A. (2013). The mathematical principles and design of the NAIS a spectrometer for the measurement of cluster ion and nanometer aerosol size distributions. *Atmospheric Measurement Techniques*, 6(4), 1061–1071.
- Moller, K. H., Berndt, T., & Kjaergaard, H. G. (2020). Atmospheric autoxidation of amines. Environmental Science and Technology, 54(18), 11087-11099.
- Oberreit, D. R., McMurry, P. H., & Hogan, C. J. (2014). Mobility analysis of 2 nm to 11 nm aerosol particles with an aspirating drift tube ion mobility spectrometer. Aerosol Science and Technology, 48(1), 108–118.
- Oberreit, D., Rawat, V. K., Larriba-Andaluz, C., Ouyang, H., McMurry, P. H., & Hogan, C. J., Jr. (2015). Analysis of heterogeneous water vapor uptake by metal iodide cluster ions via differential mobility analysis-mass spectrometry. *The Journal of Chemical Physics*, 143(10), Article 104204.
- Picache, J. A., Rose, B. S., Balinski, A., Leaptrot, K. L., Sherrod, S. D., May, J. C., & McLean, J. A. (2019). Collision cross section compendium to annotate and predict multi-omic compound identities. *Chemical Science*, 10, 983–993.
- Poschl, U. (2005). Atmospheric aerosols: Composition, transformation, climate and health effects. Angewandte Chemie International Edition in English, 44(46), 7520–7540.
- Ramanathan, V., Crutzen, P. J., Kiehl, J. T., & Rosenfeld, D. (2001). Aerosols, climate, and the hydrological cycle. Science, 294(5549), 2119-2124.
- Rappé, A. K., Casewit, C. J., Colwell, K. S., III, W. A. G., & Skiff, W. M. (1992). UFF, a full periodic table force field for molecular mechanics and molecular dynamics simulations. *Journal of the American Chemical Society*, 114, 10024–10039.
- Revercomb, H. E., & Mason, E. A. (1975). Theory of plasma chromatography/gaseous electrophoresis— a review. Analytical Chemistry, 47(7), 970-983.
- Rus, J., Moro, D., Sillero, J. A., Royuela, J., Casado, A., F, E.-M., & Fernández de la Mora, J. (2010). IMS–MS studies based on coupling a differential mobility analyzer (DMA) to commercial API–MS systems. *International Journal of Mass Spectrometry*, 298(1–3), 30–40.
- Shrivastav, V., Nahin, M., Hogan, C. J., & Larriba-Andaluz, C. (2017). Benchmark comparison for a multi-processing ion mobility calculator in the free molecular regime. *Journal of the American Society for Mass Spectrometry*, 28(8), 1540–1551.
- Spelsberg, D., & Meyer, W. (1994). Static dipole polarizabilities of N2, O2, F2, and H2O. The Journal of Chemical Physics, 101(2), 1282-1288.
- Thomas, J. M., He, S., Larriba-Andaluz, C., DePalma, J. W., Johnston, M. V., & Hogan, C. J., Jr. (2016). Ion mobility spectrometry-mass spectrometry examination of the structures, stabilities, and extents of hydration of dimethylamine-sulfuric acid clusters. *Physical Chemistry Chemical Physics*, 18(33), 22962–22972.
- von Klot, S., Peters, A., Aalto, P., Bellander, T., Berglind, N., D'Ippoliti, D., Elosua, R., Hormann, A., Kulmala, M., Lanki, T., Lowel, H., Pekkanen, J., Picciotto, S., Sunyer, J., Forastiere, F., & G.Health Effects of Particles on Susceptible Subpopulations Study. (2005). Ambient air pollution is associated with increased risk of hospital cardiac readmissions of myocardial infarction survivors in five European cities. *Circulation*, 112(20), 3073–3079.
- Wiedensohler, A., Birmili, W., Nowak, A., Sonntag, A., Weinhold, K., Merkel, M., Wehner, B., Tuch, T., Pfeifer, S., Fiebig, M., Fjäraa, A. M., Asmi, E., Sellegri, K., Depuy, R., Venzac, H., Villani, P., Laj, P., Aalto, P., Ogren, J. A., ... Bastian, S. (2012). Mobility particle size spectrometers: Harmonization of technical standards and data structure to facilitate high quality long-term observations of atmospheric particle number size distributions. *Atmospheric Measurement Techniques*, 5(3), 657-685